FULL PAPERS

Magnetic Resonance in Medicine 55:974–978 (2006)

Fast CT-PRESS-Based Spiral Chemical Shift Imaging at 3 Tesla

Dirk Mayer,* Dong-Hyun Kim, Elfar Adalsteinsson, and Daniel M. Spielman

A new sequence is presented that combines constant-time point-resolved spectroscopy (CT-PRESS) with fast spiral chemical shift imaging. It allows the acquisition of multivoxel spectra without line splitting with a minimum total measurement time of less than 5 min for a field of view of 24 cm and a nominal 1.5 × 1.5-cm^2 in-plane resolution. Measurements were performed with 17 CS encoding steps in t_1 (Δt_1 = 12.8 ms) and an average echo time of 151 ms, which was determined by simulating the CT-PRESS experiment for the spin systems of glutamate (Glu) and *myo*-inositol (mI). Signals from N-acetyl-aspartate, total creatine, choline-containing compounds (Cho), Glu, and mI were detected in a healthy volunteer with no or only minor baseline distortions within 14 min on a 3 T MR scanner. Magn Reson Med 55:974–978, 2006. © 2006 Wiley-Liss, Inc.

Key words: ^{1}H MRS; fast chemical shift imaging; effective homonuclear decoupling; J-coupling; glutamate; *myo*-inositol

While proton MR spectroscopy (MRS) is a useful, noninvasive tool that provides biochemical information about in vivo molecular processes, attempts to evaluate the spectra at clinical field strengths of 1.5 and 3 T are often hampered by severe signal overlap due to the small dispersion of the chemical shift (CS), the multiplet structure of J-coupled resonances, and line broadening caused by inhomogeneities of the local B_0 field. At higher field strengths, single-voxel short echo time (TE) MRS in combination with quantitation methods using prior knowledge has been successfully applied to measure the concentrations of up to 18 brain metabolites in vivo (1,2). Spectral editing techniques are useful for measuring a particular metabolite (3,4), but they often limit the number of resonances that can be detected simultaneously. Two-dimensional (2D) techniques such as correlation spectroscopy (COSY) increase the spectral resolution by spreading the signals of J-coupled resonances onto a plane (5,6). Although the additional spectral information is obtained at the expense of increased minimum total measurement time, this technique has been applied in vivo in both single-voxel (7–9) and CS imaging (CSI) experiments (10–13). An additional disadvantage of COSY-type experiments is a reduced sensitivity because the signals are distributed onto multiple peaks.

Another 2D technique is J-resolved MRS (14–16), which increases the spectral resolution by separating the CS and J-coupling information along two orthogonal frequency dimensions. Since the spectral width in the additional frequency dimension (SW_1) needs to cover only the spectral range of the multiplet structure of the J-coupled resonances, the method requires fewer encoding steps compared to COSY experiments. This increases the applicability of CSI versions of this technique, especially when it is combined with fast CSI methods (17–20).

Constant-time point-resolved spectroscopy (CT-PRESS) (21) has been introduced as a single-voxel technique to detect coupled resonances with high signal-to-noise ratio (SNR) by using effective homonuclear decoupling (22). It consists of a PRESS module for voxel selection and an additional refocusing pulse whose position is shifted to encode CS information along the additional time dimension (t_1). Since the whole CS range has to be sampled in CT-PRESS, it requires the same number of encoding steps as in a COSY experiment. However, it is possible to use a variant with fewer encoding steps, comparable to 2D J-resolved MRS, by undersampling the data in f_1. This does not lead to signal overlap, because all of the signals occur close to the spectral diagonal (21). Compared to 2D J-resolved MRS, CT-PRESS has the advantage that the evolution time (t_c), i.e., the TE at the central CS encoding step, can be optimized with respect to the coupling pattern and constants of the spin system of interest in order to increase the SNR of a particular peak.

Therefore, the aim of this work was to combine CT-PRESS with fast spiral CSI (23) in a new sequence that would allow the acquisition of multivoxel spectroscopic data without line splitting in acceptable scan times for clinical studies. For the presented application in the healthy human brain, the sequence was optimized for the detection of both glutamate (Glu) and *myo*-inositol (mI). As the major excitatory neurotransmitter in the central nervous system, Glu has an important role in a variety of neurological and psychiatric diseases (24–26). The function of mI is not well understood, but it is a cellular osmolite (27) and has been proposed as a marker for glial cells (28).

Richard M. Lucas Center for Magnetic Resonance Spectroscopy and Imaging, Department of Radiology, Stanford University, Stanford, California, USA.

Dong-Hyun Kim is now at the Department of Radiology, University of California–San Francisco, San Francisco, California.

Elfar Adalsteinsson is now at the Harvard-MIT Division of Health Sciences and Technology, and Department of Electrical Engineering and Computer Science, Massachusetts Institute of Technology, Cambridge, Massachusetts.

Grant sponsor: NIH; Grant numbers: CA48269; RR09784; AA12388; AG18942; Grant sponsor: Lucas Foundation.

*Correspondence to: Dirk Mayer, Lucas Center for Imaging, Department of Radiology, Stanford University, 1201 Welch Road, Stanford, CA 94305-5488. E-mail: dirk.mayer@stanford.edu

Received 3 October 2005; revised 22 December 2005; accepted 29 December 2005.

DOI 10.1002/mrm.20853

Published online 3 April 2006 in Wiley InterScience (www.interscience.wiley.com).

MATERIALS AND METHODS

Experimental

The implemented CT-PRESS spiral CSI sequence (Fig. 1) consists of five parts: 1) a three-pulse (Gaussian shape, 26 ms) CHESS module for water suppression, 2) an outer volume suppression (OVS) module (29), 3) a PRESS module (TE = 30 ms) for volume selection, 4) an additional refocusing pulse for CS encoding in t_1, and 5) a spiral readout module for combined spatial-spectral encoding in k_x, k_y, and t_2. The 3.6-ms 90° excitation pulse used in this study was a Shinar-Le Roux pulse (30) with a linear phase design. All three 5.2-ms refocusing pulses were reduced flip angle pulses (31) with a flip angle of 167°. These pulses were chosen as a compromise between reducing the RF peak power and increasing the bandwidth (i.e., reducing the CS artifact). The CS encoding pulse was shifted in increments $\Delta t_1/2$ of 6.4 ms (corresponding to an undersampling factor of 8) leading to a spectral width in f_1 of 78.125 Hz. The nominal spectral resolution in f_1 is sufficient to separate the Glu C4 resonance from signals from glutamine (Gln) and N-acetyl-aspartate (NAA) (32). We optimized the experiment for the spin systems of Glu and mI by simulating the spectroscopic part of the implemented pulse sequence for different evolution times and calculating the signal intensity of the peaks in the 1D diagonal spectra (see Data Processing below). The simulations were carried out with the full-density matrix using the GAMMA NMR simulation library (33). The CS and J-coupling constants for the metabolites were taken from Ref. 34. The CT-PRESS experiment was simulated without spectral undersampling for evolution times ranging from 127 ms to 248.6 ms with 121 CS encoding steps in t_1 (Δt_1 = 1.6 ms), 1024 complex points in t_2 at SW_2 = 2500 Hz, and ideal (infinitively short) RF pulses with the same flip angle as in the experiments. The time domain data were multiplied by exponential functions with decaying constants T_2 and T_2', respectively, to take spin-spin relaxation and B_0 inhomogeneities into account. T_2' was chosen to be 64 ms corresponding to a line width of approximately 5 Hz. Since simulations for both CT-PRESS and CT-COSY have shown that the position of a relative maximum is rather insensitive to changes in T_2 (11,32), the simulations were carried out only for a transverse relaxation constant of 200 ms for both Glu and mI. Based on the dependence of the signal intensity of both the Glu C4 resonance and the combined peak of the C[3,4] and C[1,6] protons of mI at approximately 3.6 ppm on the evolution time (Fig. 2), we chose a t_c of 151 ms for the subsequent experiments.

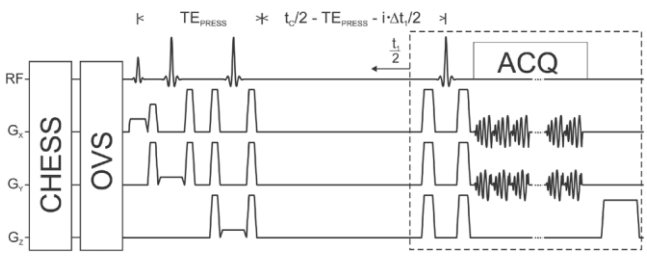

FIG. 1. RF and gradient scheme of the implemented CT-PRESS spiral CSI sequence, which was preceded by CHESS water suppression and OVS modules. CS information is encoded in t_1 by shifting the position of the last refocusing pulse ($-n_1/2 < i < n_1/2$).

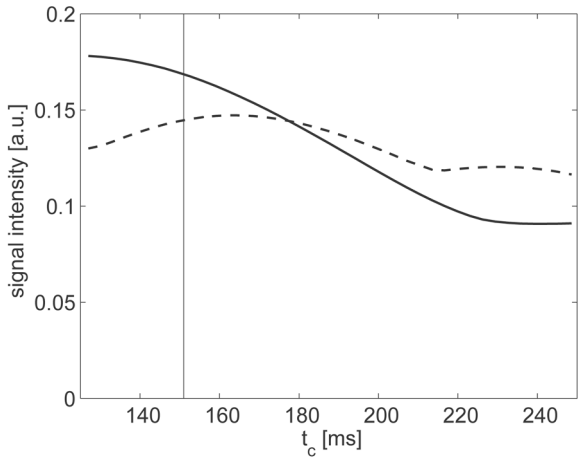

FIG. 2. Calculated signal intensity in the diagonal spectrum of the Glu C4 resonance (solid line) and the combined peak of the C[3,4] and C[1,6] protons of mI at approximately 3.6 ppm (dashed line) as a function of t_c. The vertical line marks the evolution time of 151 ms, which was used in the experiments.

Due to hardware restrictions, the maximum number of data points acquired continuously at the readout bandwidth of 250 kHz is 7168, which corresponds to a spectral resolution in f_2 of only 35 Hz or 0.3 ppm, respectively. Therefore, n_{cat} of these readout blocks were concatenated to increase the spectral resolution. Each excitation was repeated with the start of data acquisition shifted by 1.3 ms to fill the resulting gaps in the acquisition. The spiral gradient waveforms were calculated using an analytic algorithm (35), and each spiral lobe was followed by a rewinding gradient in order to return the *k*-space trajectory to the (k_x, k_y)-origin. Two spiral designs with a nominal spatial resolution of 4.5 cm^3 were tested: 1) four spatial interleaves with an FOV of 24 × 24 cm^2 for a 16 × 16 matrix and SW_2 of 1196 Hz (n_{cat} = 9), and 2) 12 spatial interleaves with an oversized FOV of 48 × 48 cm^2 for a 32 × 32 matrix and SW_2 of 1050 Hz (n_{cat} = 10). With a repetition time (TR) of 2 s and four excitations performed without data acquisition to bring the system to a steady state, the total measurement time (T_{meas}) was 4:40 min and 13:40 min for the acquisition schemes with four and 12 spatial interleaves, respectively. The spiral CSI readout module started right after the last spoiler gradient pulse of the CS encoding pulse and was shifted together with the pulse in order to increase the SNR.

All measurements were performed on a 3 T Signa MR scanner (GE Healthcare, Waukesha, WI, USA) equipped with self-shielded gradients (40 mT/m, 150 mT/m/ms). Both RF excitation and signal reception were carried out with the use of a quadrature, dome-shaped birdcage coil (36). All scans were approved by the institutional review board.

Data Processing

Gridding (37) was performed in k_x, k_y, and t_2 with an overgrid factor of 2 and a convolution kernel representing

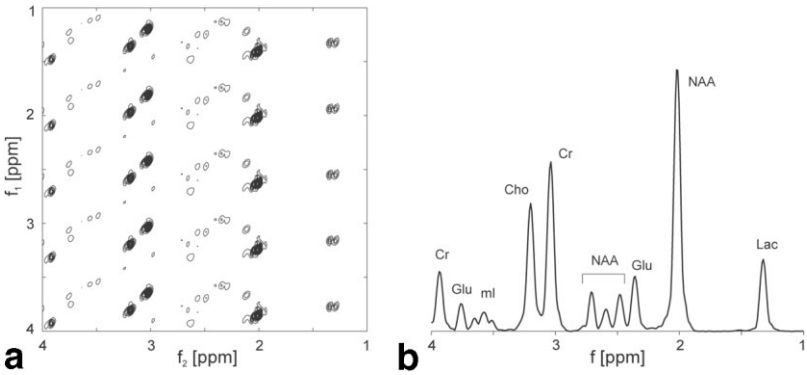

FIG. 3. (**a**) Unwrapped 2D contour plot and (**b**) corresponding diagonal spectrum (both in magnitude mode) from a single voxel within a spherical phantom filled with a solution of various brain metabolites at physiological concentration levels. Since the data are undersampled in f_1 (eightfold), the 2D contour plot has to be unwrapped in order to calculate the diagonal spectrum.

a triangular function. The data sets were apodized in both time dimensions by multiplication with sine-bell functions and zero-filling up to 1024 and 32 points, respectively, and a 3D fast Fourier transformation (FFT) was performed along k_x, k_y, and t_2. Post-density compensation was applied using an inverse cosine function. A t_1-dependent linear phase correction was applied along f_2 to correct for shifting the start of data acquisition, and the final FFT was performed along t_1. After unwrapping the 2D spectra in f_1, we calculated the diagonal spectra by integrating the spectra (magnitude mode) along f_2 within a ±13-Hz interval around the spectral diagonal.

RESULTS

The performance of the sequence was tested on a spherical phantom (17-cm inner diameter) containing the following chemicals: N-acetyl-L-aspartic acid (12.5 mM), creatine hydrate (10 mM), 3) choline chloride (3 mM), 4) mI (7.5 mM), 5) L-glutamic acid (12.5 mM), 6) DL-lactic acid (5 mM), sodium azide (0.1%), potassium phosphate (50 mM), sodium hydroxide (56 mM), and 1 ml/l Gd-DPTA (Magnevist). The PRESS module selected a 90 × 135 × 20-mm^3 volume through the center of the sphere. Figure 3 shows both the unwrapped 2D contour plot and the corresponding diagonal spectrum from a single voxel of a data set that was acquired in 4:40 min. The contour plot demonstrates the effect of the effective decoupling scheme as the line splitting due to J-coupling is suppressed in f_1. Therefore, all the signals appear as single lines in the diagonal spectrum. The peak visible in the 2D plot at (1.85, 2.1) ppm is an artifact from the residual water signal due to the gridding. However, since it is outside the integration interval, it does not affect the calculation of the diagonal spectrum.

For in vivo application of the method, a 92 × 108 × 20-mm^3 volume (axial slice orientation) was selected above the ventricles of a healthy volunteer (Fig. 4a). The map of diagonal spectra (4 ppm $\geq f \geq$ 1 ppm) from voxels completely within the preselected volume shown in Fig. 4b demonstrates the overall good spectral quality. Because of the relatively long evolution time, there are no or only minor baseline variations from macromolecule resonances or insufficient water or lipid suppression. Due to their different resonance frequencies, the position of the volume selected by the PRESS module is slightly shifted for the different metabolites. This CS artifact is the main reason for the different relative intensities of the singlet resonances of NAA, tCr, and choline-containing compounds (Cho) in the top row spectra compared to the bottom row. Figure 4c–f show the unwrapped contour plots and the corresponding diagonal spectra from voxels containing predominantly gray and white matter, respectively. Using the effective homonuclear decoupling scheme and an optimized t_c, it is possible to detect signals from both Glu and mI with high SNR despite the long average TE. While the Glu C4 resonance is well separated from NAA and Gln signals, the small glycine singlet at 3.56 ppm contributes to the mI peak at 3.6 ppm because these two signals cannot be fully separated using this technique at 3 T.

DISCUSSION AND CONCLUSIONS

The presented data show the feasibility of combining CT-PRESS with a fast spiral CSI-based technique. This allows the acquisition of multivoxel spectroscopic data without line splitting. This work demonstrates that by using effective homonuclear decoupling, compounds such as Glu and mI can be reliably measured in vivo without water or lipid baseline artifacts, which typically hamper short-TE CSI. By suppressing the line splitting, it is possible to resolve these resonances even in magnitude spectra, which usually have broader lines than absorption mode spectra. Evaluating the spectra in magnitude mode eliminates the need to phase correct the data, which is a potential source of error.

Besides suppressing the line splitting, CT-PRESS has the advantage that the timing of the sequence can be optimized to increase the SNR of a particular coupled resonance. Consequently, other resonances are detected at a less than optimal SNR. However, the reduction in SNR levels does not severely limit the ability to detect those resonances because the dependence of the signal intensity on t_c is usually a slowly varying function (see Fig. 2).

For strongly coupled spin systems, the effective homonuclear decoupling scheme leads to additional signals that have to be taken into account when the spectra are evaluated (22,32). In the diagonal spectrum these signals occur at the mean CS of the coupled resonances, and their intensities are functions of coupling constants and the chosen t_c. An example of this effect is the NAA peak at 2.58 ppm, which is caused by the strong coupling between the two resonances of the aspartate moiety of NAA at 2.49 ppm and 2.67 ppm, respectively.

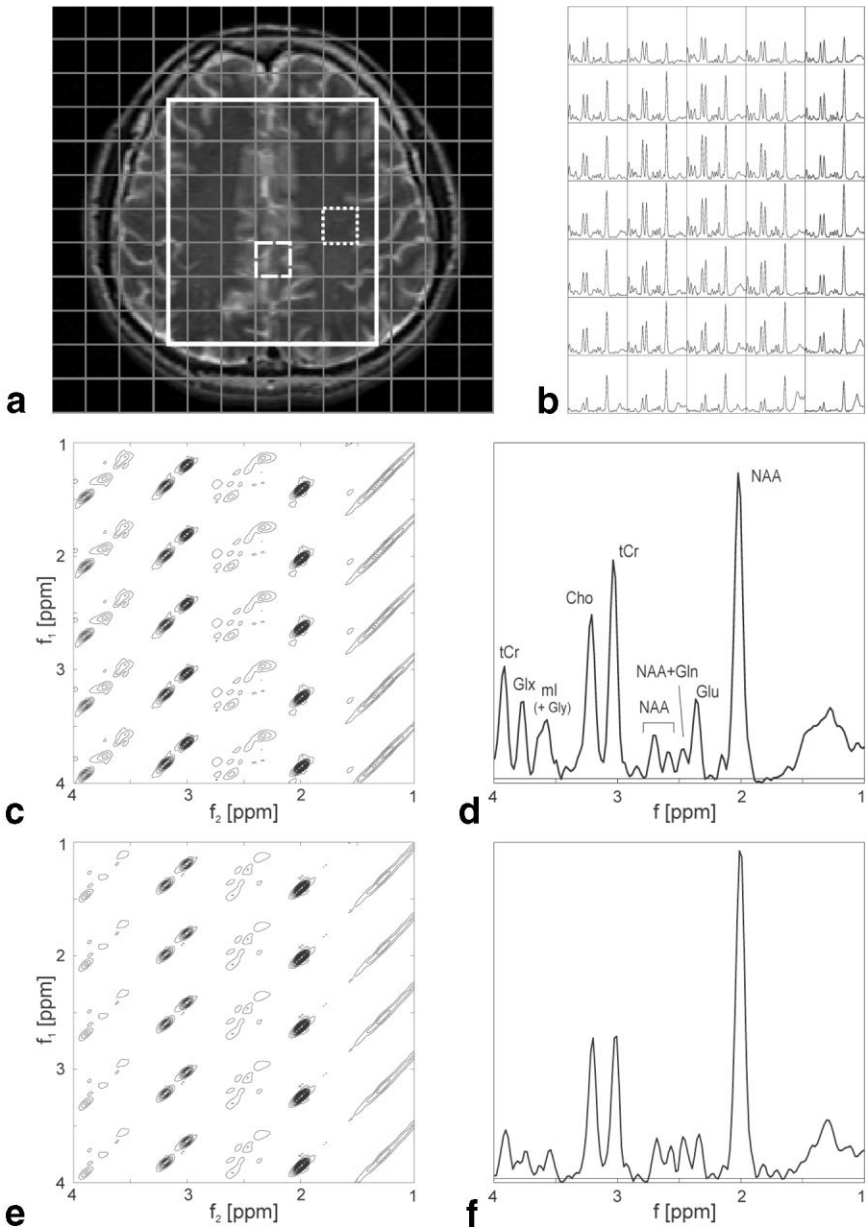

FIG. 4. **a:** High-resolution T_2-weighted fast-spin-echo water image from a healthy volunteer. The white rectangle marks the position of the volume selected by the PRESS module of the CSI sequence. **b:** Map of diagonal spectra (4 ppm $\geq f \geq$ 1 ppm) from voxels that are completely within the preselected volume. **c–f:** Unwrapped 2D contour plots and the corresponding diagonal spectra (all in magnitude mode) from voxels that contain predominantly gray (indicated by dashed square in a) and white matter (dotted square), respectively.

While the long average TE reduces baseline variations, it also leads to signal attenuation due to transverse relaxation. Hence, a more accurate knowledge of T_2 values is necessary for absolute quantitation. Since the data are acquired at different TEs, T_2 information is encoded in the data and potentially could be extracted. The effect of J-coupling during the long TE on the signal can be accounted for by using prior knowledge of the coupling constants, as has been done to optimize the evolution time to detect Glu and mI. Research into implementing an optimized multidimensional fitting algorithm to permit absolute quantitation is currently ongoing. However, the method as presented here is useful for detecting regional differences and temporal changes in the relative intensities of the metabolites.

It should be possible to extend the method to acquire 3D spatial information within total scan times of approximately 15 min by using multiple-coil arrays and parallel imaging reconstruction methods (38).

REFERENCES

1. Pfeuffer J, Tkac I, Provencher SW, Gruetter R. Toward an in vivo neurochemical profile: quantification of 18 metabolites in short-echo-time ^{1}H NMR spectra of the rat brain. J Magn Reson 1999;141:104–120.
2. Tkac I, Andersen P, Adriany G, Merkle H, Ugurbil K, Gruetter R. In vivo ^{1}H NMR spectroscopy of the human brain at 7 T. Magn Reson Med 2001;46:451–456.
3. Hetherington HP. Homo- and heteronuclear editing in proton spectroscopy. NMR: Basic Principals Prog 1992;27:179–198.
4. Allen PS, Thompson RB, Wilman AH. Metabolite-specific NMR spectroscopy in vivo. NMR Biomed 1997;10:435–444.
5. Jeener J. Ampere International Summer School, Basko Polje, Yugoslavia, 1971.
6. Aue WP, Bartholdi E, Ernst RR. Two-dimensional spectroscopy. Application to nuclear magnetic resonance. J Chem Phys 1976;64:2229–2246.

7. Berkowitz BA, Wolff SD, Balaban RS. Detection of metabolites *in vivo* using 2D proton correlated spectroscopy. J Magn Reson 1988;79:547–553.
8. Brereton IM, Galloway GJ, Rose SE, Doddrell DM. Localized two-dimensional shift correlated spectroscopy in humans at 2 Tesla. Magn Reson Med 1994;32:251–257.
9. Ryner LN, Sorenson JA, Thomas MA. 3D localized 2D NMR spectroscopy on an MRI scanner. J Magn Reson B 1995;107:126–137.
10. Ziegler A, Metzler A, Kockenberger W, Izquierdo M, Komor E, Haase A, Decorps M, von Kienlin M. Correlation-peak imaging. J Magn Reson B 1996;112:141–150.
11. Mayer D, Dreher W, Leibfritz D. Fast echo planar based correlation-peak imaging: demonstration on the rat brain in vivo. Magn Reson Med 2000;44:23–28.
12. Mayer D, Dreher W, Leibfritz D. Fast U-FLARE-based correlation-peak imaging with complete effective homonuclear decoupling. Magn Reson Med 2003;49:810–816.
13. Ziegler A, Gillet B, Beloeil JC, Macher JP, Decorps M, Nedelec JF. Localized 2D correlation spectroscopy in human brain at 3 T. MAGMA 2002;14:45–49.
14. Dreher W, Leibfritz D. On the use of two-dimensional-J NMR measurements for in vivo proton MRS: measurement of homonuclear decoupled spectra without the need for short echo times. Magn Reson Med 1995;34:331–337.
15. Ryner LN, Sorenson JA, Thomas MA. Localized 2D J-resolved 1H MR spectroscopy: strong coupling effects in vitro and in vivo. Magn Reson Imaging 1995;13:853–869.
16. Aue WP, Karhan J, Ernst RR. Homonuclear broad band decoupling and two-dimensional J-resolved NMR spectroscopy. J Chem Phys 1976;64:4226–4227.
17. Adalsteinsson E, Spielman DM. Spatially resolved two-dimensional spectroscopy. Magn Reson Med 1999;41:8–12.
18. Hiba B, Serduc R, Provent P, Farion R, Remy C, Ziegler A. 2D J-resolved spiral spectroscopic imaging at 7 T: application to mobile lipid mapping in a rat glioma. Magn Reson Med 2004;52:658–662.
19. Kim DH, Margolis D, Xing L, Daniel B, Spielman D. In vivo prostate magnetic resonance spectroscopic imaging using two-dimensional J-resolved PRESS at 3 T. Magn Reson Med 2005;53:1177–1182.
20. Srinivasan R, Cunningham C, Chen A, Vigneron D, Hurd R, Pelletier D, Nelson S. 2D spectroscopic imaging of glutamate at 3T using TE-averaged PRESS. In: Proceedings of the 13th Annual Meeting of ISMRM, Miami, FL, USA, 2005. p 724.
21. Dreher W, Leibfritz D. Detection of homonuclear decoupled in vivo proton NMR spectra using constant time chemical shift encoding: CT-PRESS. Magn Reson Imaging 1999;17:141–150.
22. Bax A, Freeman R. Investigation of complex networks of spin-spin coupling by two-dimensional NMR. J Magn Reson 1981;44:542–561.
23. Adalsteinsson E, Irarrazabal P, Topp S, Meyer C, Macovski A, Spielman DM. Volumetric spectroscopic imaging with spiral-based k-space trajectories. Magn Reson Med 1998;39:889–898.
24. Siggins GR, Martin G, Roberto M, Nie Z, Madamba S, De Lecea L. Glutamatergic transmission in opiate and alcohol dependence. Ann NY Acad Sci 2003;1003:196–211.
25. Morimoto K, Fahnestock M, Racine RJ. Kindling and status epilepticus models of epilepsy: rewiring the brain. Prog Neurobiol 2004;73:1–60.
26. Hynd MR, Scott HL, Dodd PR. Glutamate-mediated excitotoxicity and neurodegeneration in Alzheimer's disease. Neurochem Int 2004;45:583–595.
27. Nakanishi T, Turner RJ, Burg MB. Osmoregulatory changes in myo-inositol transport by renal cells. Proc Natl Acad Sci USA 1989;86:6002–6006.
28. Brand A, Richter-Landsberg C, Leibfritz D. Multinuclear NMR studies on the energy metabolism of glial and neuronal cells. Dev Neurosci 1993;15:289–298.
29. Tran TK, Vigneron DB, Sailasuta N, Tropp J, Le Roux P, Kurhanewicz J, Nelson S, Hurd R. Very selective suppression pulses for clinical MRSI studies of brain and prostate cancer. Magn Reson Med 2000;43:23–33.
30. Pauly J, Le Roux P, Nishimura D, Macovski A. Parameter relations for the Shinnar-Le Roux selective excitation pulse design algorithm. IEEE Trans Med Imaging 1991;10:53–65.
31. Raidy T, Sailasuta N, Hurd R, Pauly J. Application of reduced flip angle "180°" RF pulses in PRESS. In: Proceedings of the 3rd Annual Meeting of ISMRM, Nice, France, 1995. p 1020.
32. Mayer D, Spielman DM. Detection of glutamate in the human brain at 3 T using optimized constant time point resolved spectroscopy. Magn Reson Med 2005;54:439–442.
33. Smith SA, Levante TO, Meier BH, Ernst RR. Computer simulations in magnetic resonance. an object-oriented programming approach. J Magn Reson Ser A 1994;106:75–105.
34. Govindaraju V, Young K, Maudsley AA. Proton NMR chemical shifts and coupling constants for brain metabolites. NMR Biomed 2000;13:129–153.
35. Glover GH. Simple analytic spiral k-space algorithm. Magn Reson Med 1999;42:412–415.
36. Fitzsimmons JR, Scott JD, Peterson DM, Wolverton BL, Webster CS, Lang PJ. Integrated RF coil with stabilization for fMRI human cortex. Magn Reson Med 1997;38:15–18.
37. Jackson JI, Meyer CH, Nishimura DG, Macovski A. Selection of a convolution function for Fourier inversion using gridding [computerized tomography application]. IEEE Trans Med Imaging 1991;10:473–478.
38. Dydak U, Weiger M, Pruessmann KP, Meier D, Boesiger P. Sensitivity-encoded spectroscopic imaging. Magn Reson Med 2001;46:713–722.